ISSN: 3007-9640 DOI: https://doi.org/10.70114/acmsr.2025.5.1.P99

Constrained-Unconstrained Strategy Empowers Metastable Assemblies to Achieve Breakthrough Enhancement in Photocatalytic Hydrogen Evolution Efficiency

Yongsheng Bai[1], Shaoyue Shuai[1], Wenying Shi [1, 2 *]

[1] State Key Laboratory of Chemical Resource Engineering, Beijing University of Chemical Technology, Beijing 100029, China;

[2] Quzhou Institute for Innovation in Resource Chemical Engineering, Zhejiang 324000, China.

[a] shiwy@mail.buct.edu.cn

Abstract. Solar photocatalytic hydrogen production represents a significant development direction within the clean energy sector. Whilst symmetric organic photocatalysts offer advantages such as abundant raw materials and tunable structures, their high exciton binding energy (E_b) severely constrains the conversion efficiency from solar to hydrogen energy. This study employs 3,9-pyridinedicarboxylic acid (PDA) as a model molecule, proposing an entrapment-release engineering strategy: PDA is confined within the interlayer space of layered double hydroxides (LDH), inducing the formation of a metastable stacked structure. Upon deconfinement, this structure persists to form a supramolecular assembly (SSA). This approach generates a dipole moment exceeding 20 Debye for PDA tetramers, with internal electric field intensities tenfold higher than crystalline structures. The ionisation energy E_b drops below 50 meV. Interfacial water molecules stabilise the supramolecular assembly via hydrogen bonding, yielding a water contact angle below 30° and enhancing surface reactions. Under visible light irradiation, the optimised SSA achieves a hydrogen evolution rate of 42.83 mmol·g^{-1}·h^{-1}, significantly surpassing most organic photocatalysts. This study transforms molecular symmetry from a limiting factor into a tunable parameter, establishing a novel paradigm for organic photocatalyst design.

Keywords: Layered double hydroxides; Supramolecular assemblies; Photocatalytic hydrogen evolution

1. Introduction

With the intensification of global energy shortages and environmental pollution, developing clean, renewable hydrogen energy has become a critical direction. Solar photocatalytic hydrogen production technology, capable of directly converting solar energy into hydrogen, is regarded as a highly promising hydrogen production pathway[1–4]. While inorganic semiconductors offer superior chemical stability, they suffer from narrow visible light absorption ranges, reliance on rare-metal co-catalysts, and high photogenerated carrier recombination rates[5–7]. Organic photocatalysts, however, have become a research focus due to their advantages of abundant elements, tunable visible light absorption, and low synthesis costs. Among these, symmetric aromatic carboxylic acid molecules are widely applied in photocatalytic hydrogen production because their large π-conjugated systems can efficiently capture light energy and facilitate charge transfer. Nevertheless, symmetric organic photocatalysts commonly face the bottleneck of high exciton binding energy (E_b)[8]. For instance, pure 3,9-perylene dicarboxylic acid (PDA) crystals often exhibit E_b exceeding 100 meV. leading to non-radiative recombination of photogenerated excitons and charge separation efficiencies below 10%, severely limiting photocatalytic hydrogen evolution performance. Existing strategies to address this issue, such as constructing heterojunctions or designing donor-acceptor (D-A) molecules, offer some improvement but suffer from limitations including stringent energy level matching requirements and complex synthesis processes, while failing to fully exploit the inherent structural characteristics of symmetric molecules[9–13].

Layered double hydroxides (LDH), as two-dimensional layered materials, possess tunable interlayer spacing and excellent chemical stability[14]. Building upon this, this study employs PDA

ISSN: 3007-9640 DOI: https://doi.org/10.70114/acmsr.2025.5.1.P99
as a model molecule and proposes a confinement-deconfinement strategy: first, LDH interlayer confinement forces PDA to adopt a thermodynamically unstable tilted stacking structure; subsequently, mild-condition deconfinement preserves this structure to form a supramolecular assembly (SSA). This approach requires neither complex molecular design nor heterogeneous structure construction. Through spatial regulation alone, it alters the stacking pattern of symmetric molecules, inducing strong dipole moments and internal electric fields. This reduces E_b and enhances charge separation efficiency. Concurrently, PDA carboxyl groups form hydrogen bonds with interfacial water molecules, further stabilising the SSA and enhancing surface hydrophilicity. This study aims to elucidate the evolution of PDA stacking under LDH confinement, reveal the correlation mechanism between the electronic properties and catalytic performance of metastable SSAs, validate the regulatory role of water molecules, and transform molecular symmetry from a limiting factor into a controllable parameter. It provides experimental evidence and a novel paradigm for the design of organic photocatalysts.

2. Methods

2.1 Materials

3,9-Phenanthroline dicarboxylic acid (PDA, purity ≥ 98%), magnesium chloride hexahydrate ($MgCl_2 \cdot 6H_2O$, analytical grade), aluminium chloride hexahydrate ($AlCl_3 \cdot 6H_2O$, analytical grade), sodium hydroxide (NaOH, analytical grade) , hydrochloric acid (HCl, 37%, analytical grade), ascorbic acid (AA, analytical grade), hexahydrate chloroplatinic acid ($H_2PtCl_6 \cdot 6H_2O$, Pt ≥ 38%), all procured from Beijing Inokai Technology Co., Ltd.; deionised water was prepared in-house (purified via Milli-Q system, resistivity ≥ 18.2 MΩ · cm).

2.2 Characterization of the Materials

X-ray diffractometer (XRD, Shimadzu XRD-6000, Japan), employed for analysing crystal structures and interplanar spacings; Scanning electron microscope (SEM, Hitachi HT7800, Japan), utilised for examining material microstructures; Fluorescence spectrophotometer (FL, Hitachi F-7000, Japan), employed for measuring fluorescence spectra and exciton binding energies; Electrochemical workstation (CHI-760E, Shanghai Chenhua), for testing charge separation efficiency and internal electric field; Photocatalytic reaction system (Beijing Bofilai Technology Co., Ltd., model PLS-SXE300), equipped with a 300W xenon lamp and 420nm cut-off filter, for photocatalytic hydrogen production performance testing; Contact angle measuring instrument (Germany Kruss DSA100), for water contact angle testing.

2.3 Synthesis of Mg_3Al-Cl-LDHs

Preparation of Mg_3Al-Cl-LDH via the co-precipitation method: Add 100 mL of 1.00 M sodium chloride solution to a 500 mL four-neck flask. Under N_2 atmosphere, simultaneously add 90 mL of a mixed salt solution (Solution A) containing 7.50 mM $MgCl_2 \cdot 6H_2O$ and 2.50 mM $AlCl_3 \cdot 6H_2O$ to the flask. Solution A and 100 mL of 1.00 M sodium hydroxide solution (solution B) were simultaneously added dropwise to the flask. The reaction system was maintained at pH = 8.0 under magnetic stirring. Following completion of the addition, the mixture was aged at room temperature for 24 hours. The precipitate was collected by centrifugation (8000 rpm, 10 min), washed with deionised water to neutrality, and vacuum-dried at 60°C for 12 hours to yield Mg_3Al-Cl-LDH powder.

ISSN: 3007-9640 DOI: https://doi.org/10.70114/acmsr.2025.5.1.P99

2.4 Preparation of PDA-LDH Precursor

Preparation of PDA-LDH via ion exchange: Disperse 0.50 g Mg_3Al-Cl-LDH in 100 mL of 10 mM PDA solution. Adjust the pH to 8.5 using NaOH solution. Conduct ion exchange by stirring at 80°C for 48 hours. Following reaction completion, centrifugal washing removed free PDA (until the supernatant exhibited no green fluorescence). The product was dispersed in methanol to prepare a 20.00 $g \cdot L^{-1}$ stock solution, serving as the PDA-LDH precursor.

2.5 Preparation of PDA-based SSA

Take 100 μL of PDA-LDH stock solution, add 300 μL of 3 M HCl, and sonicate for 10 minutes in a 0°C ice bath. This process releases PDA from the LDH interlayer, forming an ordered PDA array with active extension properties. Allow the solution to stand at room temperature for 3 hours, centrifuge to collect the precipitate, and vacuum-dry at 60°C for 6 hours to obtain the PDA-based SSA.

3. Results and Discussions

Figure 1A displays the XRD diffraction patterns of Mg_3Al-Cl-LDH, PDA-LDH, and SSA. Compared to Mg_3Al-Cl-LDH, the characteristic diffraction peak of PDA-LDH shifts towards a smaller angle (2θ = 9.1°), confirming the successful insertion of PDA molecules into the two-dimensional confined space of LDH. In the XRD diffraction pattern of SSA, the characteristic LDH peaks disappear, replaced by a broadened diffraction peak (2θ = 28.3°). This indicates complete removal of the LDH template and the amorphous structure of SSA. This broadened peak corresponds to the π-π packing distance between PDA molecules. Figure 1B and 1C displays SEM images of PDA crystals and SSA. PDA crystals exhibit an irregular lamellar structure, measuring approximately 350 nm, with a smooth surface and loosely arranged molecules. In contrast, SSA adopts a one-dimensional needle-like morphology, measuring approximately 6 μm in length and 450 nm in width. This long-range ordered structure arises from the directional elongation of PDA molecules during the restriction-deregulation process, thereby facilitating the long-distance transport of photo-generated carriers.

Furthermore, the UV-Vis absorption spectra (Figure 1D) reveal that SSA exhibit broader absorption ranges and greater wavelength blue shifts compared to PDA monomers. This further indicates that LDH, acting as an energy trap, stabilises the metastable ordered PDA array and enhances intermolecular interactions, thereby facilitating the formation of supramolecular assemblies.

ISSN: 3007-9640 DOI: https://doi.org/10.70114/acmsr.2025.5.1.P99

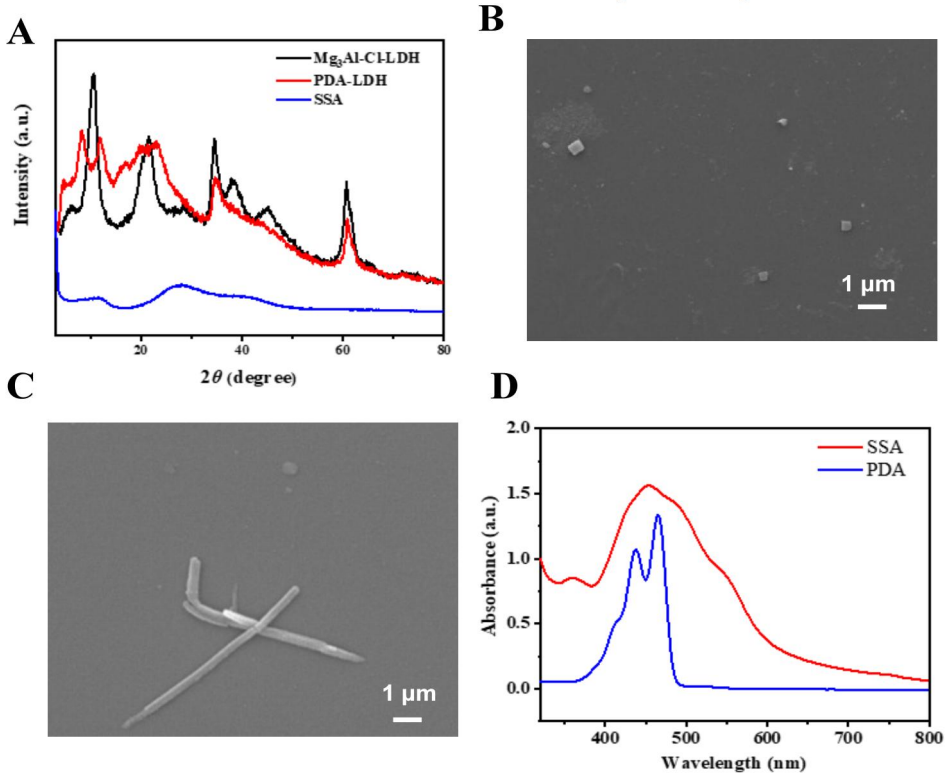

Fig. 1 (A) XRD patterns of LDH, PDA-LDH, and SSA. (B) SEM image of PDA. (C) SEM image of SSA. (D) UV-Vis absorption spectra of PTA monomer and SSA.

Measurements of the open-circuit potential (OCP) under ionic exchange field strength reveal that the PDA crystal exhibits an OCP of 78.5 mV, whereas the SSA demonstrates a markedly elevated value of 326.8 mV. Calculations indicate that the internal electric field (IEF) of SSA is 10.6 times that of the crystal. The intense electric field effect shields the Coulombic interactions between excitons, effectively reducing E_b while promoting the separation of photo-generated electron-hole pairs (Fig. 2A–D).

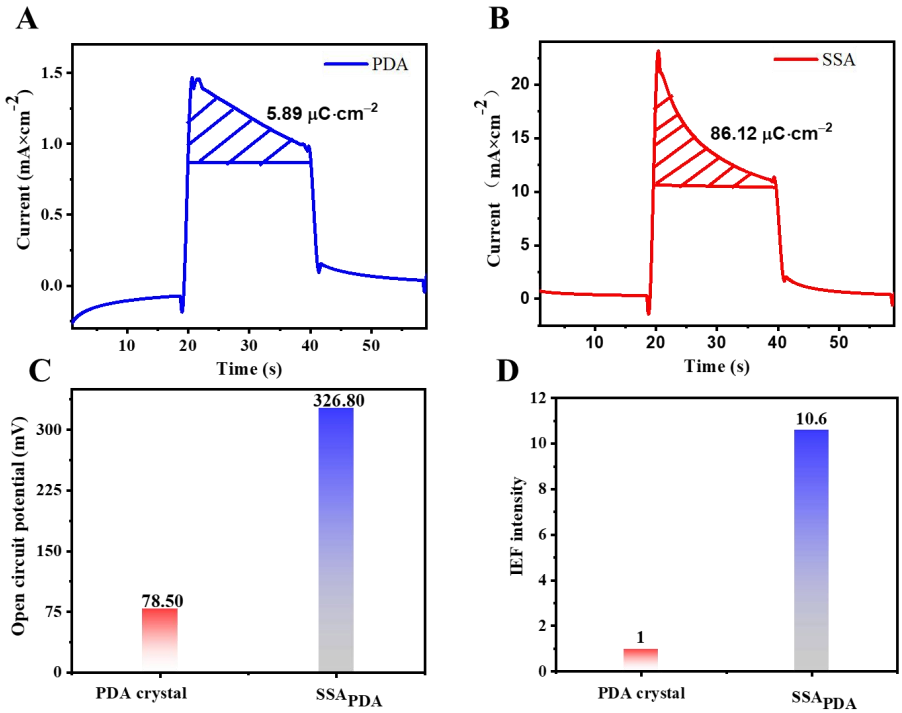

Fig. 2 The photocurrent density of (A) PDA crystal and (B) SSAPDA. (C) OCP. (D) IEF of PDA crystal and SSAPDA.

ISSN: 3007-9640 DOI: https://doi.org/10.70114/acmsr.2025.5.1.P99

Density functional theory (DFT) calculations of the dipole moment for PDA tetramers indicate that the tetramer dipole moment in PDA crystals is merely 4.8 Debye, whereas that in SSA reaches 22.3 Debye—4.6 times the crystalline value (Fig. 3A). This strong dipole moment originates from the asymmetric charge distribution resulting from the tilted stacking arrangement.

Fig. 3B and 3C display the temperature-dependent fluorescence spectra and E_b fitting curves for the SSA, respectively. The fitted E_b value of 47.3 meV falls below 50 meV and is comparable to inorganic semiconductors, thereby providing favourable conditions for highly efficient exciton separation.

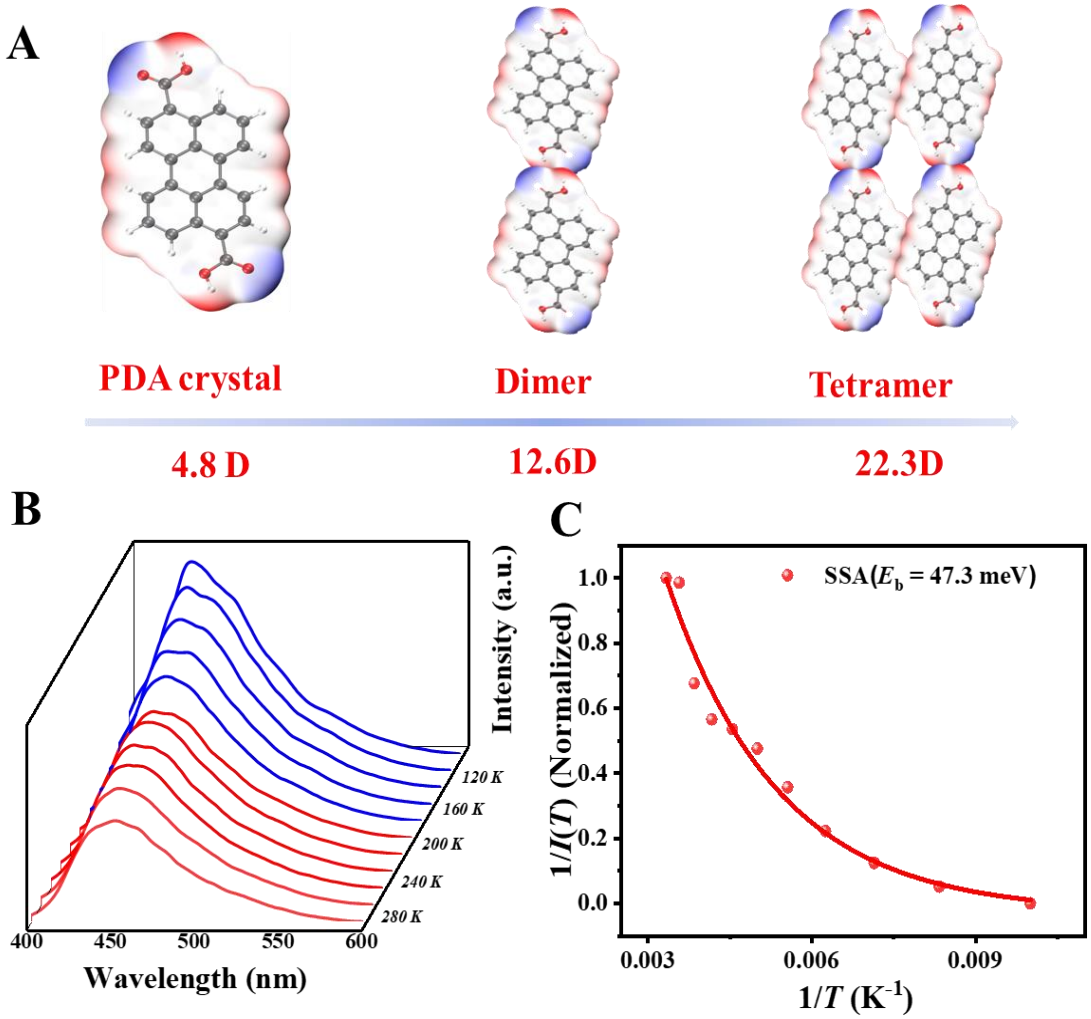

Fig. 3 (A) Dipole moment of PDA crystals, PDA dimers and PDA tetramers. Temperature-dependent (B) FL spectra and (C) FL emission intensity as a function of temperature in the 100–300 K range for SSA.

Fig. 4A and 4B presents the water contact angle test results for PDA crystals and SSA. The water contact angle of PDA crystals was 40.76°, with its hydrophobic surface limiting water molecule contact with active sites. The water contact angle of SSA decreased to 28.98°, indicating significantly enhanced hydrophilicity. The hydrophilic surface accelerates the adsorption and activation of water molecules on the material surface, thereby promoting the hydrogen evolution reaction.

ISSN: 3007-9640 DOI: https://doi.org/10.70114/acmsr.2025.5.1.P99

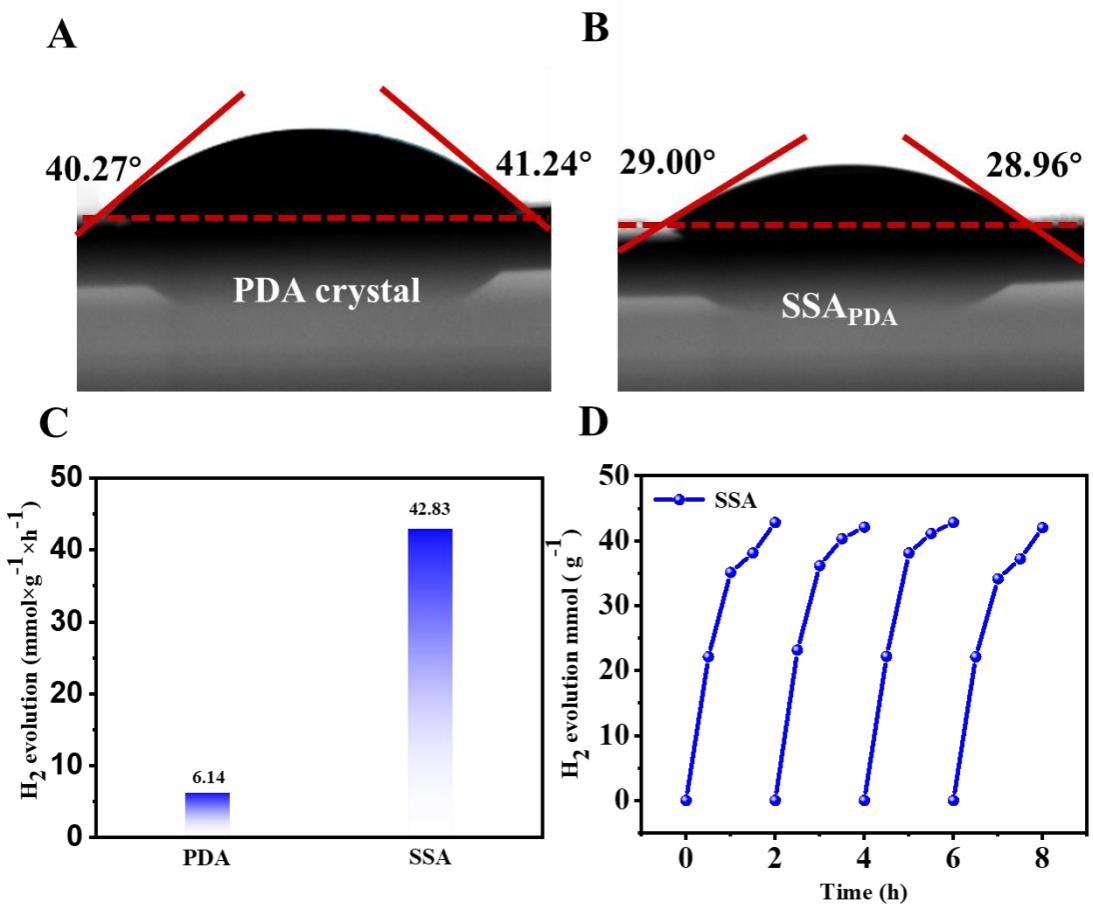

Fig. 4 Contact angle images between PDA crystals and corresponding SSA and water: (A) PDA crystals and (B) SSAPDA. (C) Photocatalytic hydrogen evolution rates of PDA crystals and PDASSA (D) Cyclic stability of hydrogen evolution from PDASSA

Fig. 4C shows the photocatalytic hydrogen evolution curves of PDA crystals and SSA under visible light. The hydrogen evolution rate of PDA crystals was only 6.14 $mmol \cdot g^{-1} \cdot h^{-1}$, whereas SSA exhibited a hydrogen evolution rate of 42.83 $mmol \cdot g^{-1} \cdot h^{-1}$, representing 6.98 times that of the crystal. Moreover, its performance significantly surpassed most reported organic photocatalysts. The stability of SSA was evaluated through cyclic hydrogen evolution experiments: after four cycles (each lasting 2 h), the hydrogen evolution rate of SSA decreased by only 5.2% (Fig. 4D). This stability is attributed to the stabilising effect of interfacial water molecules on the SSA structure via hydrogen bonding, which prevents agglomeration or decomposition of the material during the reaction process.

4. Summary

This study successfully synthesised high-performance PDA-based SSA using PDA as a model molecule through a constrained-deconstrained engineering strategy. This configuration persisted upon constraint removal, leading to the formation of needle-like SSA. The tilted stacking induces a strong dipole moment of 22.3 Debye and a substantial IEF (10.6 times that of the crystal) in PDA tetramers, reducing the E_b to 47.3 meV. Interfacial water molecules stabilise the SSA structure via hydrogen bonding, lowering the contact angle to 28.98°. This enhances surface hydrophilicity and water molecule activation efficiency, providing ample active sites for hydrogen evolution. Under visible light irradiation, the SSA achieves a hydrogen evolution rate of 42.83 $mmol \cdot g^{-1} \cdot h^{-1}$, maintaining stable performance after four cycles—significantly outperforming most organic photocatalysts. This study demonstrates that the confinement-deconfinement strategy transforms the

ISSN: 3007-9640 DOI: https://doi.org/10.70114/acmsr.2025.5.1.P99
symmetry of symmetric molecules from a limiting factor into a tunable parameter. It establishes a universal paradigm for designing high-performance organic photocatalysts and pioneers new pathways for applying two-dimensional confinement techniques in energy catalysis.

Acknowledgements

The National Natural Science Foundation of China (22171018 and 22438007), the Beijing Municipal Natural Science Foundation (2242012).

References

[1] Hai Xiao, Fang Liqi, Xiong Minghui, et al. Charge density modulation of pyrene-related small molecules by nitrogen heteroatoms precisely regulates photocatalytic generation of hydrogen. ACS Nano, 2023, 17(20): 20570–20579.
[2] Song Hui, Luo Shunqin, Huang Hengming, et al. Solar-driven hydrogen production: Recent advances, challenges, and future perspectives. ACS Energy Letters, 2022, 7(3): 1043–1065.
[3] Tarhan C, Çil M A. A study on hydrogen, the clean energy of the future: Hydrogen storage methods. Journal of Energy Storage, 2021, 40: 102676.
[4] Dawood F, Anda M, Shafiullah G M. Hydrogen production for energy: An overview. International Journal of Hydrogen Energy, 2020, 45(7): 3847–3869.
[5] Xu Yucheng, Zheng Jiaxin, et al. Consecutive charging of a perylene bisimide dye by multistep low-energy solar-light-induced electron transfer towards H_2 evolution. Angewandte Chemie International Edition, 2020, 59(26): 10363–10367.
[6] Wu Shuhong, Li Chao, Wang Ying, et al. The keto-switched photocatalysis of reconstructed covalent organic frameworks for efficient hydrogen evolution. Angewandte Chemie International Edition, 2023, 62(36): e202309026.
[7] Wu Shuhong, Cheng Xiuyan, Huang Haowei, et al. End group-induced ultrafast exciton dissociation of supramolecular perylene monoimide nanoribbons for efficient photocatalytic hydrogen evolution. Small, 2025, 21(14): 2408140.
[8] Zhu Xiaolin, Jia Yihui, Liu Yuhan, et al. Enhancing built-in electric fields via molecular symmetry modulation in supramolecular photocatalysts for highly efficient photocatalytic hydrogen evolution. Angewandte Chemie International Edition, 2024, 63(26): e202405962.
[9] Lee M M S, Xu Wenhan, Zheng Liang, et al. Ultrafast discrimination of gram-positive bacteria and highly efficient photodynamic antibacterial therapy using near-infrared photosensitizer with aggregation-induced emission characteristics. Biomaterials, 2020, 230: 119582.
[10] Fahmeed S, Deborah S, Ankit J, et al. Peptide-Based Supramolecular Systems Chemistry, 2021, 121(22): 13869–13914.
[11] Chen Songbo, Zhuo Yuling, Wang Xin, et al. Advances of layered double hydroxide electrocatalysts for high-current-density alkaline water/seawater splitting. Coordination Chemistry Reviews, 2024, 510(1): 215832.
[12] Khan A A, Tahir M, Khan N. Layered double hydroxide for photocatalytic application toward CO_2 reduction and water splitting: Recent advances, synthesis, heterojunction formation, challenges, and future directions. Applied Physics Reviews, 2025, 12(1): 011313.
[13] Li Lei, Soyhan I, Warszawik E, et al. Layered double hydroxides: Recent progress and promising perspectives toward biomedical applications. Advanced Science, 2024, 11(20): 2306035.
[14] Yang Minggang, Qiu Shi, et al. Nir-responsive TiO_2 biometasurfaces: Toward in situ photodynamic antibacterial therapy for biomedical implants. Advanced Materials, 2022, 34(6): 2106314.